Experimental Time-Optimal Universal Control of Spin Qubits in Solids

Jianpei Geng,[1] Yang Wu,[1] Xiaoting Wang,[2,3] Kebiao Xu,[1] Fazhan Shi,[1,4] Yijin Xie,[1] Xing Rong,[1,4,*] and Jiangfeng Du[1,4,†]

[1]*CAS Key Laboratory of Microscale Magnetic Resonance and Department of Modern Physics, University of Science and Technology of China, Hefei 230026, China*

[2]*Hearne Institute for Theoretical Physics, Department of Physics and Astronomy, Louisiana State University, Baton Rouge, Louisiana 70803, USA*

[3]*Research Laboratory of Electronics, Massachusetts Institute of Technology, Cambridge, Massachusetts 02139, USA*

[4]*Synergetic Innovation Center of Quantum Information and Quantum Physics, University of Science and Technology of China, Hefei 230026, China*

(Received 7 April 2016; published 19 October 2016)

Quantum control of systems plays an important role in modern science and technology. The ultimate goal of quantum control is to achieve high-fidelity universal control in a time-optimal way. Although high-fidelity universal control has been reported in various quantum systems, experimental implementation of time-optimal universal control remains elusive. Here, we report the experimental realization of time-optimal universal control of spin qubits in diamond. By generalizing a recent method for solving quantum brachistochrone equations [X. Wang *et al.*, Phys. Rev. Lett. **114**, 170501 (2015)], we obtained accurate minimum-time protocols for multiple qubits with fixed qubit interactions and a constrained control field. Single- and two-qubit time-optimal gates are experimentally implemented with fidelities of 99% obtained via quantum process tomography. Our work provides a time-optimal route to achieve accurate quantum control and unlocks new capabilities for the emerging field of time-optimal control in general quantum systems.

DOI: 10.1103/PhysRevLett.117.170501

Time-optimal control (TOC), including the famous examples of the brachistochrone problem [1] and the Zermelo navigation problem [2], has been widely investigated for over three centuries. TOC of quantum systems has recently attracted great interest due to the rapid development of quantum information processing and quantum metrology. Because the ever-present noise from the environment degrades quantum states or operations over time, generating the fastest possible evolution by TOC becomes a preferable choice for realizing precise quantum control in the presence of noise. To obtain accurate TOC protocols is difficult because both the fidelity and time should be optimized. Analytical methods utilizing the Pontryagin maximum principle or the geometry of the unitary group are applicable only to specific problems and constraints [3–10]. Recently, the quantum brachistochrone equation (QBE) has been proposed to provide a general framework for finding time-optimal state evolutions or unitary operations [11–18]. The QBE has been applied to some cases where analytic solutions exist [15–17]. For problems where the QBE cannot be analytically solved, an effective numerical method has been developed [18]. The relationship between TOC and gate complexity has also been explored [19,20]. Experimental TOC has been implemented only in single-qubit systems [21–23], while experimental time-optimal universal control, which requires universal single-qubit gates as well as a nontrivial two-qubit gate, has not been reported.

Here, we demonstrate the first experimental time-optimal universal control of a two-qubit system, which consists of an electron spin and a nuclear spin of a nitrogen-vacancy (NV) center in diamond. High-fidelity single- and two-qubit gates are realized with fidelities of 99% obtained via quantum process tomography. Our results show that TOC provides a novel route to achieve precise universal quantum control. The approach to realize time-optimal control of multiple qubits can be applied to other quantum systems.

As shown in Fig. 1, the quantum system is driven by the Hamiltonian $H(t)$, which is described by the Schrödinger equation $\dot{U} = -iH(t)U$, with boundary conditions $U(0) = I$ and $U(T) = U_F$ (we set $\hbar = 1$). Different Hamiltonians $H(t)$ make the evolutions of the system follow different paths (labeled by Γ_i) to the same unitary operation U_F. The path with the minimal time cost can be obtained by solving the QBE [12] together with the Schrödinger equation. The QBE is written as

$$\dot{F} = -i[H, F], \tag{1}$$

where $F = \partial L_C/\partial H$ and $L_C = \sum_j \lambda_j f_j(H)$, with λ_j the Lagrange multiplier. One physically relevant constraint is the finite energy bandwidth described as $f_0(H) \equiv [\mathrm{Tr}(H^2) - E^2]/2 = 0$, where E is a constant. Reference [18] provides a method to obtain the accurate minimum-time protocol by solving the QBE.

In realistic physical systems, part of the Hamiltonian H is usually time independent (e.g., fixed couplings between spin qubits), and the reasonable constraint for the energy is actually for the time variable part (e.g., the shaped

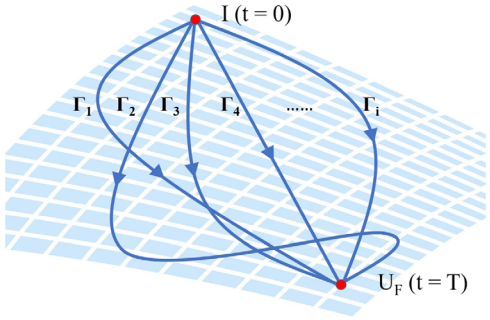

FIG. 1. Schematic representation of quantum TOC. Blue lines represent paths of quantum evolution in the $SU(2^n)$ operator space, where n stands for the number of qubits. To realize a target evolution operator U_F at $t = T$ starting from the identity operator I at $t = 0$, there are several choices of evolution path $\Gamma_i (i = 1, 2, \ldots)$. The goal of TOC is to figure out which evolution costs the minimum time T.

microwave pulse with bounded power). These have been recently recognized and investigated as the quantum Zermelo navigation problem [24,25]. The original QBE is not able to provide a solution to this problem directly. Here, we rewrite the Hamiltonian $H(t)$ as $H = H_0 + H_c(t)$, where the drift Hamiltonian H_0 stands for the time invariable part and $H_c(t)$ stands for the control Hamiltonian. The drift Hamiltonian H_0 can be the fixed spin couplings or nonzero constant external magnetic field. The control Hamiltonian $H_c(t)$ can be a controllable external magnetic field or adjustable couplings between qubits. The constraint of the finite energy bandwidth is modified to $f_0(H_c) = 0$. Then, the TOC of multiple qubits, which is experimentally feasible, can be obtained by solving the QBE with the mentioned improvements (see Sec. II in the Supplemental Material [26]). This method can be taken as the generalization of the method in Ref. [18], which is the case of $H_0 = 0$.

We experimentally demonstrate TOC of single- and two-qubit systems on an NV center in diamond. The NV center is composed of an electron spin and a nitrogen nuclear spin. A static magnetic field of about 500 G is applied along the NV symmetry axis ([1 1 1] crystal axis) and removes the degeneracy between the $|m_S = +1\rangle$ and $|m_S = -1\rangle$ electron spin states. Under such a magnetic field, the spin state of the NV center is effectively polarized to $|m_S = 0, m_I = +1\rangle$ when a 532 nm laser pulse is applied [27]. Microwave pulses driving the electron spin transition $|m_S = 0\rangle$ to $|m_S = -1\rangle$ and radio-frequency pulses driving the nuclear spin transition $|m_I = +1\rangle$ to $|m_I = 0\rangle$ are utilized to manipulate the spin states. The $|m_S = +1\rangle$ electron spin level and $|m_I = -1\rangle$ nuclear spin level remain idle due to large detuning. TOC is demonstrated on the two-qubit system composed by $|m_S = 0, m_I = +1\rangle$, $|m_S = -1, m_I = +1\rangle$, $|m_S = 0, m_I = 0\rangle$, and $|m_S = -1, m_I = 0\rangle$ without considering the other spin levels (see Sec. I and Fig. S1 in the Supplemental Material [26]).

The experiment was implemented on an NV center in [100] face bulk diamond. The nitrogen concentration in the diamond was less than 5 ppb, and the abundance of ^{13}C was at the natural level of 1.1%. The NV center was optically addressed by a home-built confocal microscope. Spin-state initialization and detection of the NV center were realized with a 532 nm green laser controlled by an acousto-optic modulator (ISOMET, power leakage ratio $\sim 1/1000$). To preserve the NV center's longitudinal relaxation time from laser leakage effects, the laser beam was passed twice through the acousto-optic modulator before going through an oil objective (Olympus, PLAPON 60*O, NA 1.42). The phonon sideband fluorescence (wavelength 650–800 nm) went through the same oil objective and was collected by an avalanche photodiode (Perkin Elmer, SPCM-AQRH-14) with a counter card. A solid immersion lens was created around the NV center to increase the fluorescence collection efficiency. The magnetic field was provided by a permanent magnet and aligned by monitoring the variation of fluorescence counts. The spin states of the NV center were manipulated with microwave and radio-frequency pulses. The microwave and radio-frequency pulses were generated by an arbitrary waveform generator (Keysight M8190A), amplified individually with power amplifiers (Mini Circuits ZHL-30W-252-S+ for microwave pulses and LZY-22+ for radio-frequency pulses), and combined with a diplexer (Marki DPX-1). An ultrabroadband coplanar waveguide with 15 GHz bandwidth was designed and fabricated to feed the microwave and radio-frequency pulses.

Universal control of a single qubit requires the ability to realize rotations around two different axes of the Bloch sphere. The evolution operator is denoted with $R(\hat{\mathbf{n}}, \theta)$, corresponding to a rotation of angle θ around axis $\hat{\mathbf{n}} = \hat{\mathbf{x}} \sin\gamma \cos\varphi + \hat{\mathbf{y}} \sin\gamma \sin\varphi + \hat{\mathbf{z}} \cos\gamma$. The method to realize TOC gates, which rotate the quantum states along two different axes, is detailed in Sec. II in the Supplemental Material [26]. We take a target unitary transformation $R(\hat{\mathbf{z}}, \theta)$ on the electron spin qubit as an example. In the rotating frame, $H_0 = 2\pi\delta S_z$, $H_c(t) = 2\pi\nu_1[\cos\phi(t) S_x + \sin\phi(t) S_y]$, where S_x, S_y, and S_z are effective spin operators of the electron spin qubit, δ is the detuning term, $\nu_1 > 0$ stands for the amplitude of the microwave pulse, and $\phi(t)$ is the phase of microwave pulse. The control Hamiltonian H_c satisfies two constraints, which are $f_0(H_c) \equiv [\mathrm{Tr}(H_c^2) - 2\pi^2\nu_1^2]/2 = 0$ and $f_1(H_c) \equiv \mathrm{Tr}(H_c S_z) = 0$. The solution to the QBE is $\phi(t) = 2\pi\eta t + \phi(0)$, where η is a constant. Then, the detailed parameters of the control Hamiltonian [e.g., η and $\phi(t)$] and the minimum evolution time T can be obtained by further solving the Schrödinger equation. By following the procedure described above, we can derive the explicit analytical solutions to the TOC for realizing $R(\hat{\mathbf{z}}, \theta)$. Without loss of generality, we present the analytical solution when $\delta \geq 0$ and $\theta \in [0, 2\pi)$. If $\theta < \pi(1 + \sqrt{3}\delta/\nu_1)$, the minimum evolution time

$T = [\delta(\theta/2\pi - 1) + \sqrt{\nu_1^2 + \delta^2 - \nu_1^2(\theta/2\pi - 1)^2}]/(\nu_1^2 + \delta^2)$; otherwise, the minimum evolution time becomes $T = [\delta\theta/2\pi + \sqrt{\nu_1^2 + \delta^2 - \nu_1^2(\theta/2\pi)^2}]/(\nu_1^2 + \delta^2)$. The minimum evolution time T versus θ and δ/ν_1 is shown in Supplemental Fig. S2 [26]. The case when $\delta \neq 0$ is of importance to those systems where it is challenging to adjust the detuning, such as the singlet-triplet spin qubit in a double-quantum-dot system [28,29]. When $\delta = 0$, our result reduces to that in Ref. [7].

The realization of a target $R(\hat{\mathbf{z}}, \theta), \theta \in (0, \pi]$ when $\delta = 0$ is taken as an example to compare the time cost between the derived TOC and a nonoptimized evolution path with Euler rotation: $R(\hat{\mathbf{z}}, \theta) = R(\hat{\mathbf{x}}, \pi/2)R(\hat{\mathbf{y}}, \theta)R(-\hat{\mathbf{x}}, \pi/2)$. The experimental amplitude of control field is set to be $\nu_1 = 5$ MHz. Theoretical comparison of the time cost for gate operations between TOC and Euler rotation is shown in Fig. 2(a). It is clear that the time cost with TOC is considerably shorter than that with Euler rotation for all the rotation angles. We experimentally implement the target gate operators $R(\hat{\mathbf{z}}, \pi/8)$, $R(\hat{\mathbf{z}}, \pi/4)$, $R(\hat{\mathbf{z}}, \pi/2)$, and $R(\hat{\mathbf{z}}, \pi)$ with both methods. Figure 2(b) shows the comparison of the experimental gate time. The time durations for gate operations with TOC are 69.6, 96.8, 132.3, and 173.2 ns, which are 42.9, 28.1, 17.7, and 26.8 ns shorter than those with Euler rotation, respectively. Figure 2(c) shows the state evolution during $R(\hat{\mathbf{z}}, \pi)$. The initial state is prepared to $(|m_s = 0\rangle + i|m_s = -1\rangle)/\sqrt{2}$. We performed measurements of $\langle S_y \rangle$ and $\langle S_z \rangle$ on the states during the evolution. As shown in Fig. 2(c), the target evolution of $R(\hat{\mathbf{z}}, \pi)$ is realized at 173.2 ns with TOC and at 200 ns with Euler rotation. All the gate fidelities [30] are measured to be above 0.99 via quantum process tomography [31].

The case when $\delta \neq 0$ has also been experimentally implemented. Both $R(\hat{\mathbf{z}}, \theta)$ and $R(\hat{\mathbf{x}}, \theta)$ with various values of θ have been demonstrated. Furthermore, time-optimal universal single-qubit control with other constraints on H_c is also experimentally demonstrated. The implementations are characterized utilizing quantum process tomography (see Sec. III in the Supplemental Material [26]). The experimental results for the cases are presented in Sec. II, Fig. S3, Fig. S4, and Table I of the Supplemental Material [26]. Our results show the universality of our approach to perform time-optimal universal control for a single qubit.

Universal control of qubits also requires a nontrivial two-qubit gate [32]. In our experiment, we demonstrate a controlled-U gate with

$$U_c = \begin{pmatrix} 1 & 0 & 0 & 0 \\ 0 & 0 & 0 & 1 \\ 0 & 0 & 1 & 0 \\ 0 & -1 & 0 & 0 \end{pmatrix}, \quad (2)$$

which is also a nontrivial two-qubit gate [32]. In our experiment, we have demonstrated this two-qubit gate in a time-optimal way with the system consisting of the electron and nuclear spins. Electron (nuclear) spin states $|m_S = 0\rangle$ and $|m_S = -1\rangle$ ($|m_I = +1\rangle$ and $|m_I = 0\rangle$) are encoded as the electron (nuclear) spin qubit. The quantum state of the two-qubit system is denoted as $|m_S, m_I\rangle$, with corresponding population denoted as P_{m_S,m_I} hereafter. The drift Hamiltonian $H_0 = 2\pi A S_z I_z$ is the hyperfine coupling between the spins, where I_z is the effective spin operator of the nuclear spin qubit and the hyperfine coupling strength is $A = -2.16$ MHz. We consider a model in which only controls with bounded strength on the electron spin are applied, while the control Hamiltonian takes the form $H_c(t) = 2\pi\nu_1[\cos\phi(t)S_x + \sin\phi(t)S_y]$. The strength of the control field ν_1 is set to 2.5 MHz. The constraints on the control Hamiltonian can be described by $f_0(H_c) = 0$ and $f_k(H_C) \equiv \mathrm{Tr}(H_C B_k) = 0$, where $\{B_k\} = \{I_x, I_y, I_z, S_xI_x, S_xI_y, S_xI_z, S_yI_x, S_yI_y, S_yI_z, S_z, S_zI_x, S_zI_y, S_zI_z\}$. The target evolution operator is a controlled unitary gate which flips the electron spin qubit iff the nuclear spin

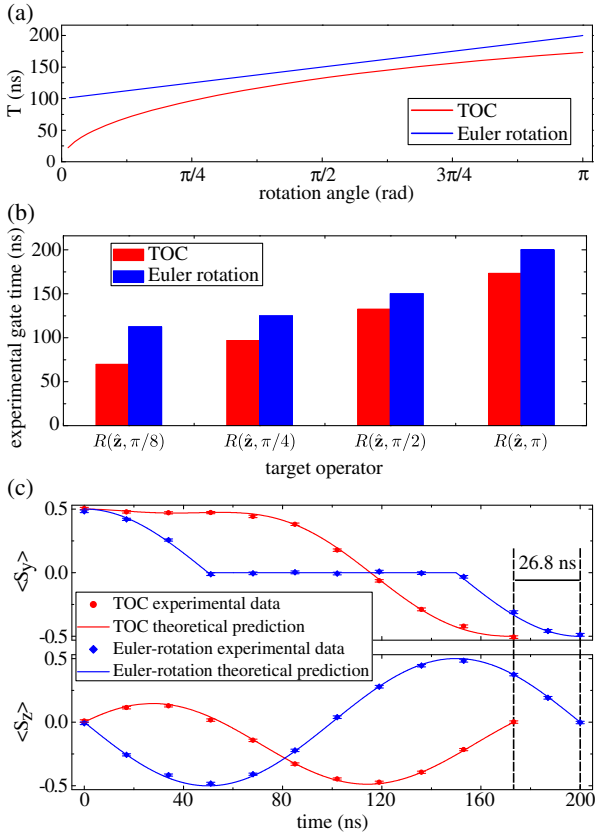

FIG. 2. Comparison on time costs for target gate operator $R(\hat{\mathbf{z}}, \theta)$ between the derived TOC and the Euler rotations. The parameters are set to be $\delta = 0$ and $\nu_1 = 5$ MHz. (a) Theoretical comparison on time with $\theta \in (0, \pi]$. (b) Comparison of experimental gate time for $\theta = \pi/8, \pi/4, \pi/2$, and π. The gate time for TOC is considerably shorter than that for Euler rotation. (c) State evolutions during $R(\hat{\mathbf{z}}, \pi)$ with TOC and Euler rotation. The initial state is $(|m_s = 0\rangle + i|m_s = -1\rangle)/\sqrt{2}$. The gate time of TOC is 26.8 ns shorter than that of Euler rotation.

qubit is in the state $|m_I = 0\rangle$. The time-optimal control Hamiltonian is obtained by numerically solving the QBE together with the Schrödinger equation (see Sec. II in the Supplemental Material [26]). If the dephasing effect and the imperfection of the control field are taken into account [33], the theoretical fidelity of U_c is estimated to be 0.9933. The detailed experimental pulse for time-optimal control and the fidelity estimation are included in Sec. II and Fig. S5 in the Supplemental Material [26]. The time duration of the controlled-U gate with TOC is 446 ns. A conventional method to implement the controlled-U gate with the constraint control field is to apply a selective pulse [34,35]. With $\nu_1 = 2.5$ MHz (the same as that in TOC), the time duration to implement the controlled-U gate with a selective pulse is 612.4 ns (see Sec. II in the Supplemental Material [26]), which is more than 160 ns longer than that with TOC.

Figure 3 shows the state evolutions under U_c via TOC. In Figs. 3(a) and 3(b), the initial states are prepared into $|0,1\rangle$ and $|0,0\rangle$, respectively. The left panel of Fig. 3(a) [Fig. 3(b)] shows the state trajectory of the electron spin qubit on the Bloch sphere, while the nuclear spin state is $|m_I = +1\rangle$ [$|m_I = 0\rangle$]. It is clear that the electron spin qubit is flipped to the state $|-1\rangle$ with the nuclear spin qubit in $|m_I = 0\rangle$, and the state of the electron spin qubit returns to the state $|0\rangle$ with the nuclear spin qubit in $|m_I = +1\rangle$. In the right panels of Figs. 3(a) and 3(b), experimental populations of $|0, m_I\rangle$ and $|-1, m_I\rangle$ (i.e., P_{0,m_I} and P_{-1,m_I}) during the U_c gate are recorded. The experimental results represented by symbols are in agreement with theoretical predictions represented as lines. The small deviation from 1 (0) of P_{0,m_I} (P_{-1,m_I}) at $t = 0$ is due to imperfect polarization of the electron spin (about 0.95, which is measured with sequences described in Sec. IV and Fig. S6 in the Supplemental Material [26]).

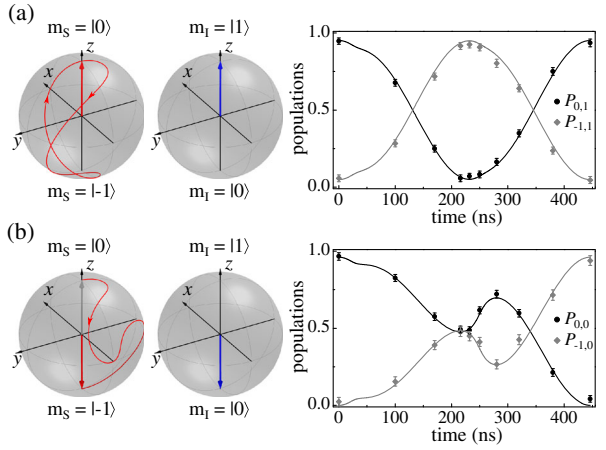

FIG. 3. State trajectories under the two-qubit controlled-U gate by TOC with initial states (a) $|0,1\rangle$ and (b) $|0,0\rangle$. The left panels show the state evolutions of the nuclear and electron spins on the Bloch spheres. When the nuclear spin qubit is in the state $|1\rangle$ ($|0\rangle$) labeled by the blue arrows, the electron spin qubit undergoes the paths labeled by red lines to the state $|0\rangle$ ($|-1\rangle$). The right panels show the experimental dynamics of state populations P_{0,m_I} (black circles) and P_{-1,m_I} (grey diamonds), and lines are theoretical predictions of the populations. The error bars on the data points are the standard deviations from the mean.

We further perform quantum process tomography (see Sec. III in the Supplemental Material [26]) to characterize the U_c gate. A set of 16 initial states is prepared, after which the U_c is applied, and quantum state tomography is applied to reconstruct the final state corresponding to each initial state. With the information of the 16 final states, the process matrix χ is determined in the Pauli basis $\{\sigma_i \otimes \sigma_j\}$, where $\sigma_{i(j)} \in \{I, X, Y, Z\}$, I is the identity operator, and $X = \sigma_x$, $Y = \sigma_y$, and $Z = \sigma_z$ are Pauli operators. Figure 4 shows the real and imaginary parts of the experimental process matrix. The average gate fidelity of the two-qubit gate in our experiment is 0.99(1), which reaches the threshold of fault-tolerant quantum computations [36]. The shortest possible time duration of the gate operation by TOC is advantageous to high fidelity due to the reduction of the dephasing effect. The relatively small strength of the control field also contributes to the high fidelity, as the noise induced from the control field is proportional to the control field [33,37].

Discussion.—Manipulation of quantum systems is of fundamental significance in quantum computing [31], quantum metrology [38], and high-resolution spectroscopy [39–41]. It is desirable to achieve universal control with high fidelity and in a minimal time interval in the presence of decoherence. High-fidelity universal control has been reported in various quantum systems, including trapped ions [42], superconducting circuits [36], NV centers in diamond [33,43], and spins in silicon [44,45]. However, experimental demonstration of universal control, when high fidelity and minimal time are satisfied simultaneously, were not achieved in previous work. We have realized the time-optimal universal control of the two-qubit system in diamond with high fidelity. Our results provide an experimental validation of TOC casting a high-fidelity control operation on multiqubit

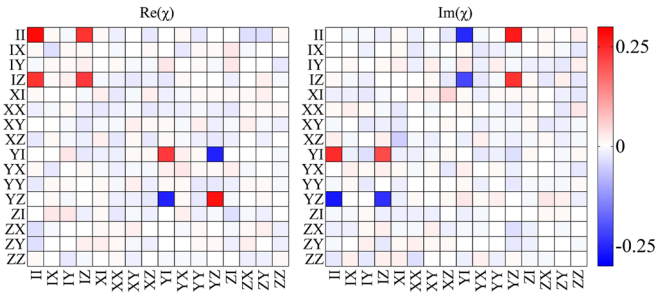

FIG. 4. Quantum process tomography for the controlled-U gate by TOC. The left and right panels are the real and imaginary parts of the reconstructed process matrix χ. The error bar of each point is about 0.01 due to the statistics of photon counts. An average gate fidelity of 0.99(1) can be obtained from the process matrix.

systems. The approach developed in this work to realize accurate minimum-time control of multiqubits can be applied to other important physical systems.

We are grateful to C. K. Duan and C. Y. Ju for valuable discussions. This work was supported by the National Basic Research Program of China (Grants No. 2013CB921800 and No. 2016YFB0501603), the National Natural Science Foundation of China (Grants No. 11227901, No. 31470835, and No. 11275183) and the Strategic Priority Research Program (B) of the CAS (Grant No. XDB01030400). F. S. and X. R. thank the Youth Innovation Promotion Association of Chinese Academy of Sciences for support. X. W. is supported by NSF Project No. CCF-1350397.

J. G. and Y. W. contributed equally to this work.

*xrong@ustc.edu.cn
†djf@ustc.edu.cn

[1] H. J. Sussmann and J. C. Willems, IEEE Control Syst. Mag. **17**, 32 (1997).
[2] E. Zermelo, Z. Angew. Math. Mech. **11**, 114 (1931).
[3] N. Khaneja, R. Brockett, and S. J. Glaser, Phys. Rev. A **63**, 032308 (2001).
[4] N. Khaneja, S. J. Glaser, and R. Brockett, Phys. Rev. A **65**, 032301 (2002).
[5] H. Yuan and N. Khaneja, Phys. Rev. A **72**, 040301 (2005).
[6] R. Fisher, H. Yuan, A. Spörl, and S. Glaser, Phys. Rev. A **79**, 042304 (2009).
[7] A. D. Boozer, Phys. Rev. A **85**, 012317 (2012).
[8] G. C. Hegerfeldt, Phys. Rev. Lett. **111**, 260501 (2013).
[9] A. Garon, S. J. Glaser, and D. Sugny, Phys. Rev. A **88**, 043422 (2013).
[10] H. Yuan, R. Zeier, N. Pomplun, S. J. Glaser, and N. Khaneja, Phys. Rev. A **92**, 053414 (2015).
[11] A. Carlini, A. Hosoya, T. Koike, and Y. Okudaira, Phys. Rev. Lett. **96**, 060503 (2006).
[12] A. Carlini, A. Hosoya, T. Koike, and Y. Okudaira, Phys. Rev. A **75**, 042308 (2007).
[13] Y. Okudaira, Ph.D. thesis, Tokyo Institute of Technology, 2008.
[14] A. T. Rezakhani, W.-J. Kuo, A. Hamma, D. A. Lidar, and P. Zanardi, Phys. Rev. Lett. **103**, 080502 (2009).
[15] A. Carlini, A. Hosoya, T. Koike, and Y. Okudaira, J. Phys. A **44**, 145302 (2011).
[16] A. Carlini and T. Koike, Phys. Rev. A **86**, 054302 (2012).
[17] A. Carlini and T. Koike, J. Phys. A **46**, 045307 (2013).
[18] X. Wang, M. Allegra, K. Jacobs, S. Lloyd, C. Lupo, and M. Mohseni, Phys. Rev. Lett. **114**, 170501 (2015).
[19] M. A. Nielsen, M. R. Dowling, M. Gu, and A. C. Doherty, Science **311**, 1133 (2006).
[20] T. Koike and Y. Okudaira, Phys. Rev. A **82**, 042305 (2010).
[21] M. Lapert, Y. Zhang, M. Braun, S. J. Glaser, and D. Sugny, Phys. Rev. Lett. **104**, 083001 (2010).
[22] M. G. Bason, M. Viteau, N. Malossi, P. Huillery, E. Arimondo, D. Ciampini, R. Fazio, V. Giovannetti, R. Mannella, and O. Morsch, Nat. Phys. **8**, 147 (2012).
[23] C. Avinadav, R. Fischer, P. London, and D. Gershoni, Phys. Rev. B **89**, 245311 (2014).
[24] D. C. Brody and D. M. Meier, Phys. Rev. Lett. **114**, 100502 (2015).
[25] B. Russell and S. Stepney, Phys. Rev. A **90**, 012303 (2014).
[26] See Supplemental Material at http://link.aps.org/supplemental/10.1103/PhysRevLett.117.170501 for details of the calculations and experimental procedures.
[27] V. Jacques, P. Neumann, J. Beck, M. Markham, D. Twitchen, J. Meijer, F. Kaiser, G. Balasubramanian, F. Jelezko, and J. Wrachtrup, Phys. Rev. Lett. **102**, 057403 (2009).
[28] S. Foletti, H. Bluhm, D. Mahalu, V. Umansky, and A. Yacoby, Nat. Phys. **5**, 903 (2009).
[29] X. Wang, L. S. Bishop, J. P. Kestner, E. Barnes, K. Sun, and S. Das Sarma, Nat. Commun. **3**, 997 (2012).
[30] M. A. Nielsen, Phys. Lett. A **303**, 249 (2002).
[31] M. A. Nielsen and I. L. Chuang, *Quantum Computation and Quantum Information* (Cambridge University Press, Cambridge, England, 2000).
[32] J. A. Jones and D. Jaksch, *Quantum Information, Computation and Communication* (Cambridge University Press, Cambridge, England, 2012).
[33] X. Rong, J. Geng, F. Shi, Y. Liu, K. Xu, W. Ma, F. Kong, Z. Jiang, Y. Wu, and J. Du, Nat. Commun. **6**, 8748 (2015).
[34] K. Dorai, Arvind, and A. Kumar, Phys. Rev. A **61**, 042306 (2000).
[35] T. S. Mahesh, K. Dorai, Arvind, and A. Kumar, J. Magn. Reson. **148**, 95 (2001).
[36] R. Barends *et al.*, Nature (London) **508**, 500 (2014).
[37] X. Rong, J. Geng, Z. Wang, Q. Zhang, C. Ju, F. Shi, C.-K. Duan, and J. Du, Phys. Rev. Lett. **112**, 050503 (2014).
[38] V. Giovannetti, S. Lloyd, and L. Maccone, Phys. Rev. Lett. **96**, 010401 (2006).
[39] P. O. Schmidt, T. Rosenband, C. Langer, W. M. Itano, J. C. Bergquist, and D. J. Wineland, Science **309**, 749 (2005).
[40] J. R. Maze *et al.*, Nature (London) **455**, 644 (2008).
[41] G. Balasubramanian *et al.*, Nature (London) **455**, 648 (2008).
[42] J. Benhelm, G. Kirchmair, C. F. Roos, and R. Blatt, Nat. Phys. **4**, 463 (2008).
[43] T. van der Sar, Z. H. Wang, M. S. Blok, H. Bernien, T. H. Taminiau, D. M. Toyli, D. A. Lidar, D. D. Awschalom, R. Hanson, and V. V. Dobrovitski, Nature (London) **484**, 82 (2012).
[44] J. J. Pla, K. Y. Tan, J. P. Dehollain, W. H. Lim, J. J. L. Morton, F. A. Zwanenburg, D. N. Jamieson, A. S. Dzurak, and A. Morello, Nature (London) **496**, 334 (2013).
[45] M. Veldhorst *et al.*, Nature (London) **526**, 410 (2015).